JMB

Available online at www.sciencedirect.com

ScienceDirect

ELSEVIER

Mechanical Unbinding of Aβ Peptides from Amyloid Fibrils

E. Prabhu Raman[1], Takako Takeda[1], Valeri Barsegov[2] and Dmitri K. Klimov[1]*

[1]*Department of Bioinformatics and Computational Biology, George Mason University, Manassas, VA 20110, USA*

[2]*Department of Chemistry, University of Massachusetts Lowell, Lowell, MA 01854, USA*

Using the experimental structures of Aβ amyloid fibrils and all-atom molecular dynamics, we study the force-induced unbinding of Aβ peptides from the fibril. We show that the mechanical dissociation of Aβ peptides is highly anisotropic and proceeds *via* different pathways when force is applied in parallel or perpendicular direction with respect to the fibril axis. The threshold forces associated with lateral unbinding of Aβ peptides exceed those observed during the mechanical dissociation along the fibril axis. In addition, Aβ fibrils are found to be brittle in the lateral direction of unbinding and soft along the fibril axis. Lateral mechanical unbinding and the unbinding along the fibril axis load different types of fibril interactions. Lateral unbinding is primarily determined by the cooperative rupture of fibril backbone hydrogen bonds. The unbinding along the fibril axis largely depends on the interpeptide Lys–Asp electrostatic contacts and the hydrophobic interactions formed by the Aβ C terminal. Due to universality of the amyloid β structure, the anisotropic mechanical dissociation observed for Aβ fibrils is likely to be applicable to other amyloid assemblies. The estimates of equilibrium forces required to dissociate Aβ peptide from the amyloid fibril suggest that these supramolecular structures are mechanically stronger than most protein domains.

© 2007 Elsevier Ltd. All rights reserved.

Edited by D. Case

Introduction

It is now well recognized that many protein sequences have a propensity to assemble into amyloid fibrils under appropriate external conditions.[1] A common sequence-independent feature of amyloids is an extensive β-sheet structure formed by fibrillized polypeptides and stabilized by the network of backbone hydrogen bonds (HBs).[2] A polypeptide amino acid sequence determines the specific arrangement of chains in β-sheets and overall three-dimensional organization of fibrils.[3–9] From the perspective of biology and biotechnology, an important characteristic of amyloid assemblies is their remarkable stability against denaturation. As a result, their formation is essentially irreversible under physiological conditions.[10]

The precise molecular organization of amyloid fibrils has long remained elusive. Recently, solid state NMR experiments have revealed a parallel in-registry arrangement† of Alzheimer's Aβ peptides in amyloid fibrils.[11–13] Using experimentally derived constraints 3D structures have been obtained for various Aβ species, including Aβ$_{10-35}$, Aβ$_{1-40}$, and Aβ$_{1-42}$.[3,5,6,14–16]

In particular, the study of Petkova *et al.*[5] has demonstrated that Aβ fibril protofilament consists of four laminated β-sheets (Fig. 1). The structural unit of the protofilament, which is replicated along the fibril axis, includes two Aβ peptides (e.g., F1 and

*Corresponding author. E-mail address:
dklimov@gmu.edu.

Abbreviations used: MD, molecular dynamics; AFM, atomic force microscopy; SMD, steered molecular dynamics; WT, wild type; CHC, central hydrophobic cluster; Ig, immunoglobulin; SBC, spherical boundary condition; HB, hydrogen bond; LD, Langevin dynamics.

† A parallel in-registry arrangement of peptides in β-sheet means that the residue i from one peptide matches the same residue i from the other peptide.

F2 in Fig. 1). One of the peptides (F2) contributes its β-strands β₁ and β₂ (Fig. 1d) to the upper pair of β-sheets and the other (F1) to the lower pair of β sheets. An interesting feature of the structure in Fig. 1 is a staggering shift along the fibril axis of the inner β-sheets (formed by β2 strands) relative to the outer β-sheets. This structural feature makes the edges of Aβ fibril distinct. The computational efforts in elucidating Aβ amyloid conformations have been recently reviewed.[17]
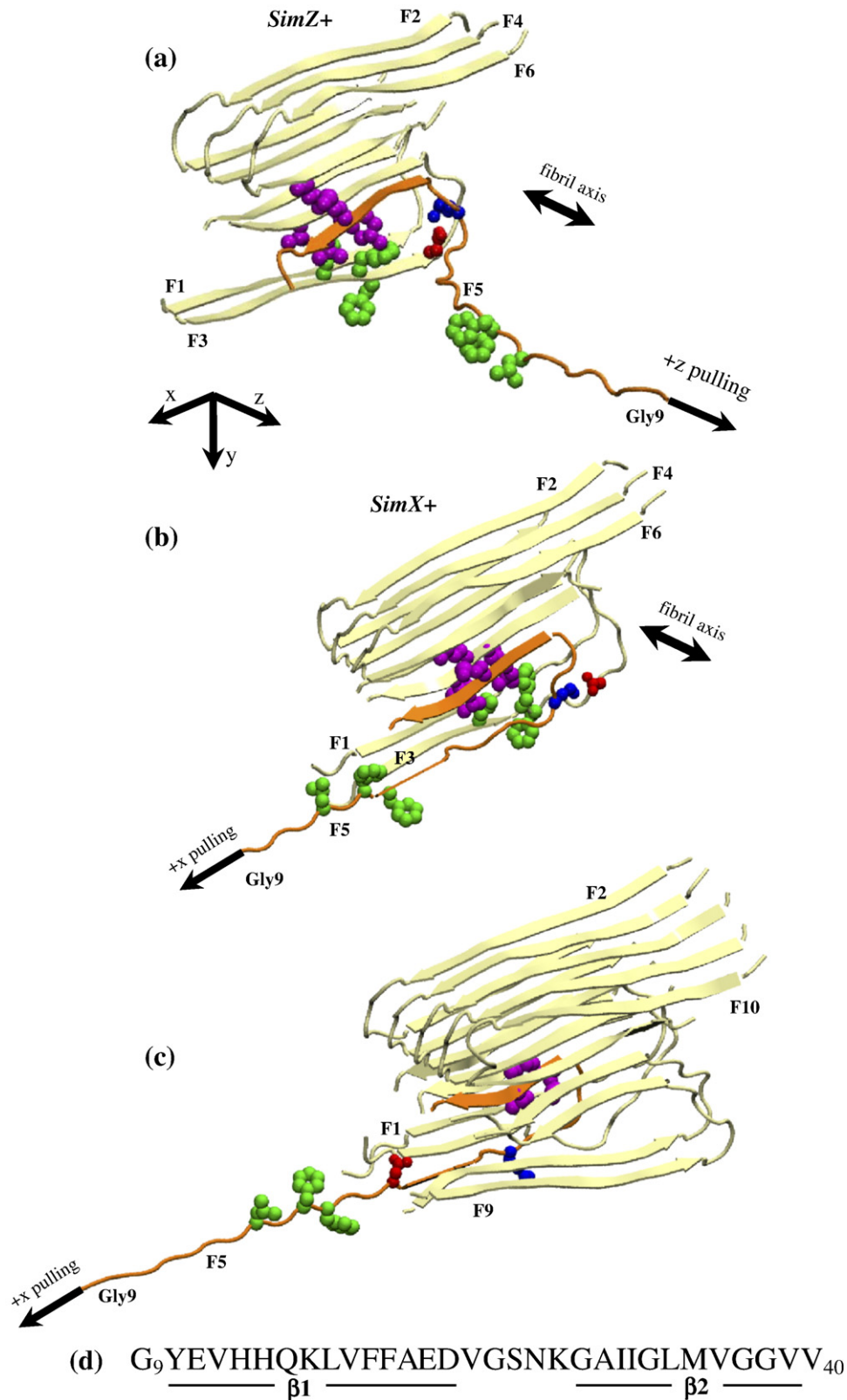

(d) G_9YEVHHQKLVFFAEDVGSNKGAIIGLMVGGVV$_{40}$
$\underline{}$ β1 $\underline{}$ $\underline{}$ β2 $\underline{}$

Fig. 1 (*legend on next page*)

It is important to investigate the stability amyloid fibrils against a variety of external factors. For example, thermal fluctuations in Aβ fibril structure have been investigated by explicit solvent molecular dynamics (MD) simulations.[18] The MD simulations of temperature-induced dissociation of the amyloid fibrils formed by Aβ fragment Aβ$_{16-22}$ have also been performed.[19] Another possibility is to examine the mechanical stability of amyloid structures against force-induced dissociation. The first atomic force microscopy (AFM) experimental studies probing their mechanical properties have already been reported.[20–26] For example, the force-induced dissociation of α-synuclein dimers grafted to a surface has been studied.[20] For the pulling speed of $v_p = 1$ μm/s the typical unbinding force was about 100 pN. Other AFM experiments probed the mechanical stability of surface-adsorbed Aβ dimers.[23] It was found that the average force of breaking the dimer's β structure is about 300 pN at the pulling speed of 0.25 μm/s. Compared to α-synuclein, Aβ peptides are longer. Additionally, Aβ dimers were incubated at low pH to induce the formation of β-structure. These two factors are the likely cause for higher mechanical stability of Aβ dimers. The mechanical dissociation of mature Aβ$_{1-40}$ fibrils deposited on a glass surface was also probed.[22] The experiments suggested that the entire Aβ protofilament is peeled away from the tethered fibril. However, despite the growing number of experimental AFM studies it is still difficult to pinpoint the specific structural transitions in individual polypeptide chains or to identify the interactions that define the mechanical strength of amyloid structure.

In the past, steered molecular dynamics (SMD) simulations[27,28] were instrumental in mapping the mechanical unfolding of proteins and provided testable predictions for AFM experiments.[29–35] One may expect that SMD simulations probing the force-induced (mechanical) dissociation of amyloid fibrils at atomic resolution may also complement AFM experiments and facilitate their interpretation. In this paper, we use SMD to study the force-induced unbinding of individual Aβ peptides from the amyloid fibril. We established that the properties of Aβ fibril against mechanical perturbation are highly anisotropic and different directions of force application load different types of intrafibril interactions. Due to universality of amyloid β-structure organization, the anisotropic mechanical dissocia-

tion reported here may be applicable not only to Aβ fibrils, but also to other amyloid assemblies. Using our simulations and available experimental data, we compare the mechanical stabilities of amyloid fibrils and protein domains.

Results

As described in Methods, we have generated two sets of SMD trajectories. Six independent trajectories (SimZ+ simulations) probed the mechanical unbinding of the edge peptide F5 along the direction parallel with the fibril axis (Fig. 1a). Six trajectories from SimX+ simulations studied the force-induced unbinding in the direction perpendicular to the fibril axis (Fig. 1b). Both sets of simulations were initiated with the state in which all peptides, including F5, adopt a fibril conformation (Methods). SimZ+ and SimX+ result in complete unbinding of the peptide F5 from the fibril. Below we provide the detailed analysis of these simulations.

Mechanical unbinding of Aβ peptides along the fibril axis

Figure 2a displays the disruption of fibril backbone HBs formed by F5 with the extension z in a typical SimZ+ trajectory (for the definition of extension, see Methods). HBs are disrupted in an "unzipping" manner, in which each HB becomes sequentially loaded with tension and broken as F5 is peeled away from the fibril (Fig. 1a). There are two stages in the rupture of fibril HBs (see inset to Fig. 2a). The first is associated with the unzipping of the strand β1 (residues Tyr10 to Asp23 in Fig. 1d) at the extension $z \lesssim 50$ Å, while the second is related to the unbinding of β2 (Gly29 to Val39) at $z \gtrsim 70$ Å. The loss of side-chain hydrophobic contacts (see Methods) mirrors the disruption of the fibril HB network (cf. Fig. 2a and b). Figure 2b shows that before unbinding the strand β1 forms relatively few hydrophobic interactions (mainly at the positions Leu17 and Phe20). For example, the average number of hydrophobic contacts per residue in β1 before unbinding is 1.5. In contrast, a typical hydrophobic residue from the strand β2 maintains, on average, 2.4 contacts with the fibril before unbinding. The anchor of hydrophobic interactions in β2 is Leu34, which forms up to five hydrophobic contacts. As we

Fig. 1. (a, b) Mechanical unbinding of the edge peptide F5 (in orange) from the Aβ$_{9-40}$ fibril hexamer consisting of the peptides F1–F6. The retaining point[55] (see Methods) coupled with the F5 N-terminal residue Gly9 moves with the constant speed along the fibril axis (SimZ+ simulations, shown in a) or in the lateral direction along the x-axis (SimX+ simulations, shown in b). The force generated in the spring coupling Gly9 and the retaining point reflects the mechanical resistance of Aβ peptide against dissociation. (c) Mechanical unbinding of the peptide F5 located in the middle of the 10-mer Aβ$_{9-40}$ fibril fragment. In (a)–(c), the CHC residues (Leu17, Phe19, Phe20) and the C-terminal residues (Leu34, Met35, Val36) are shown in green and magenta, respectively. Charged residues forming intermolecular salt bridges (Asp23, Lys28) are shown in red and blue, respectively. In (a) and (b), these residues are shown in the peptides F3 and F5. In (c), they are shown in F5 only. The panels (a)–(c) display the snapshots from pulling trajectories. The peptides F1 and F2 in (a) and (b) and F1, F2, F9, and F10 in (c) are constrained to their fibril positions. All other peptides are free. For clarity, the solvating water sphere is not shown. The structure of Aβ$_{9-40}$ fibril protofilament is derived from solid-state NMR measurements.[5] The figure is prepared using VMD.[59] (d) Sequence of Aβ$_{9-40}$ peptide and the allocation of the strands β1 and β2.
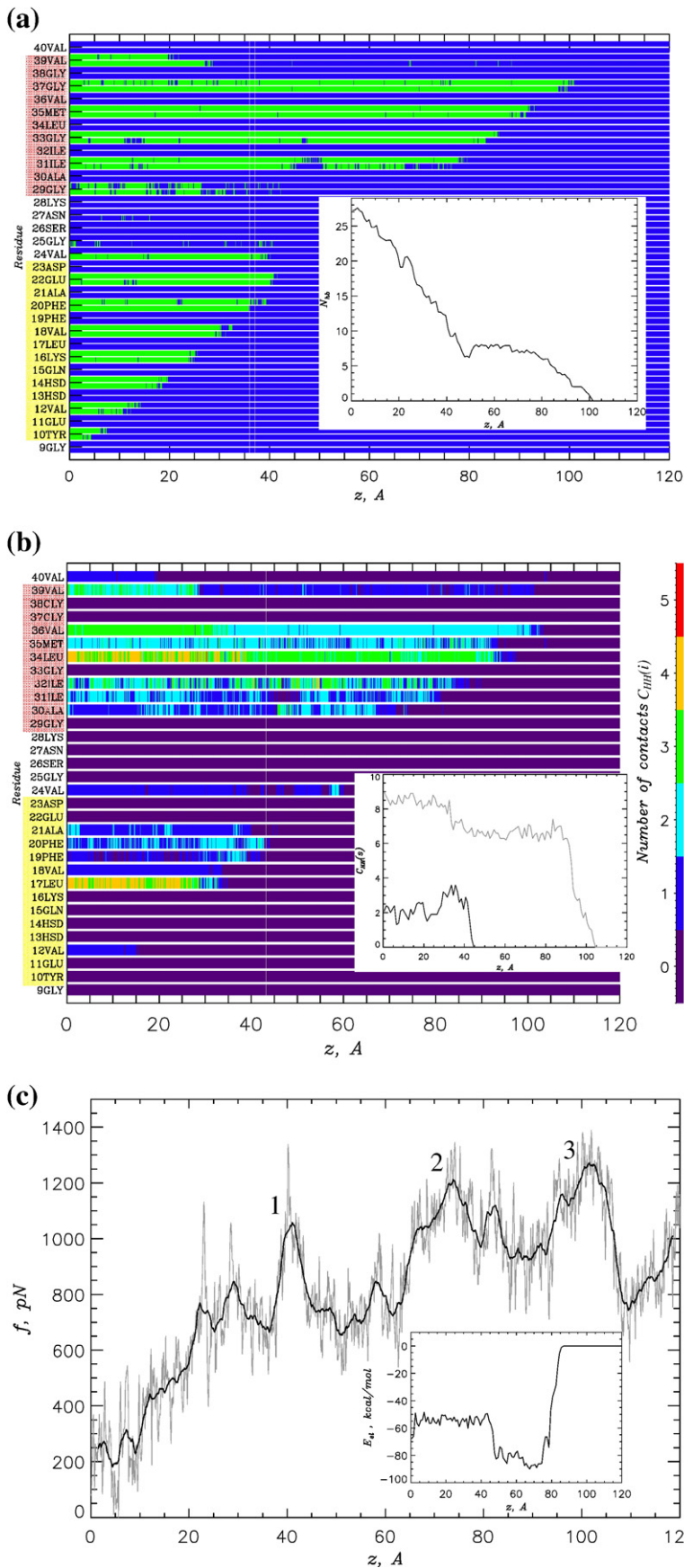
(a)

(b)

(c)

Fig. 2. (a) The dynamics of force-induced unzipping of the fibril in-registry backbone HBs between F5 and the fibril in SimZ+ trajectory. For each F5 residue there are two horizontal bars, monitoring flickering of HBs formed by NH or CO backbone groups. Green and blue code "on" and "off" states, respectively. The inset displays the total number of backbone (in- and off-registry) HBs, $N_{hb}(z)$, formed by F5 *versus* extension z. (b) The force-induced breakage of hydrophobic side-chain contacts formed by the residues in F5 *versus* extension z. The colors code the number of hydrophobic contacts $C_{HH}(i)$ formed by residue i according to the color scale on the right. $C_{HH}(i)$ includes interpeptide and nonlocal intrapeptide contacts (with the sequence separation of at least 5). The inset shows the number of hydrophobic contacts $C_{HH}(s)$ formed by the CHC phenylalanines (s=Phe19-Phe20, in black) and by the C-terminal hydrophobic patch (s=Leu34-Met35-Val36, in grey). In panels (a) and (b), the residues from the β-strands β1 and β2 are placed in yellow and pink boxes, respectively. (c) The force–extension curve $f(z)$ (in grey) describing the unbinding of the edge peptide F5 in the direction parallel with the Aβ fibril axis (Fig. 1a). The thick black line represents the force smoothed using the sliding window of Δz=3 Å. The amplitudes of force peaks are measured using the smoothed force. Peaks 1–3 are attributed to the rupture of CHC interactions, Lys–Asp interactions, and the hydrophobic tether formed by the C terminus. The inset shows the energy of electrostatic interactions $E_{el}(z)$ between the charged side chains of Lys28 (F5) and Asp23 (F3). $E_{el}(z)$ is smoothed with the sliding window of Δz=1 Å.

show below, these structural properties have profound impact on the mechanical stability of Aβ fibril (see Discussion).

Figure 2c presents the dependence of the force resisting the unbinding of F5 on the extension, $f(z)$. The plot reveals three characteristic peaks associated with structural transitions during mechanical unbinding. The peak at $z \approx 40$ Å (peak 1, ≈ 1000 pN) is primarily related to the disruption of hydrophobic interactions. Indeed, a steep decrease in the number of hydrophobic contacts formed by the peptide F5 is observed at $z \approx 40$ Å (Fig. 2b). Further examination indicates that at this extension two aromatic residues, Phe19 and Phe20, lose all their contacts with the fibril peptide F3 (see inset to Fig. 2b). Due to large structural fluctuations in the β1 strand compared to those observed in β2, the force peak 1 is small relative to other peaks in Fig. 2c (see Discussion).

The force peak 2 at $z \approx 75$ Å with the amplitude of ≈ 1200 pN is primarily caused by loading and disruption of the intermolecular salt bridge between Lys28(F5) and Asp23(F3) (Fig. 1a). The inset to Fig. 2c demonstrates that peak 2 approximately coincides with the sharp increase in the energy of electrostatic interactions $E_{el}(t)$ between Lys28(F5) and Asp23(F3). Peak 3 with the amplitude of ≈ 1300 pN occurs at $z \approx 100$ Å and is related to the unbinding of the patch of C-terminal hydrophobic residues (Leu34, Met35, Val36). The inset to Fig. 2b shows that roughly seven hydrophobic contacts formed by this patch are cooperatively disrupted in the interval $90 < z < 100$ Å.

To map the unbinding pathway, we plot the average unbinding force $<f(z)>$ obtained from six independent SimZ+ simulations (Fig. 3). The average force–extension curve $<f(z)>$ is strikingly similar to the force $f(z)$ in Fig. 2c. Indeed, although the

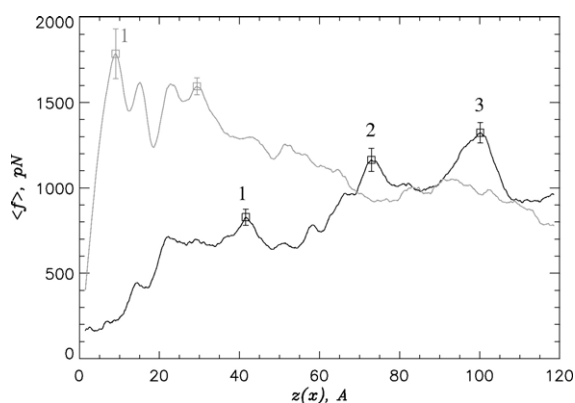**Fig. 3.** The average unbinding force $<f>$ as a function of the extension z for SimZ+ simulations (in black) or the extension x for SimX+ simulations (in grey). The force $<f>$ is averaged over six independent trajectories and smoothed using the sliding window of 3 Å. The errors in the amplitudes of force peaks are shown. Distinct SimZ+ and SimX+ force "fingerprints" indicate that the mechanical unbinding is highly anisotropic. The major force peaks are marked by numbers.

amplitudes of the force peaks in SimZ+ trajectories vary, their key features are conserved. For example, most SimZ+ trajectories contain three force peaks similar to those in Fig. 2c.

The analysis of the SimZ+ trajectory in Fig. 2 suggests that there are several key interactions that determine the mechanical stability of Aβ fibril. To provide a direct test, which will assess their contributions to the force–extension curve in Fig. 3, we studied the mechanical unbinding of F5 mutants (see Methods). Each mutant differs from the wild-type (WT) F5 by the deletion of specific set of interactions. For each mutant we repeated SimZ+ simulations and computed force–extension plots $<f(z)>$. Figure 4a compares $<f(z)>$ for the WT and the mutant M1, in which the C-terminal hydrophobic patch is deleted. The substitution of the residues Leu34, Met35, and Val36 with glycines completely eliminates the peak 3 without affecting the amplitudes and positions of other peaks. The comparison of the WT and the mutant M2 is presented in Fig. 4b. This figure suggests that the deletion of three central hydrophobic cluster (CHC) residues (Leu17, Phe19, Phe20) eliminates peak 1 but leaves peaks 2 and 3 largely intact.

The importance of Lys28–Asp23 intermolecular interactions is tested using the mutant M3, in which the charge on the Lys28 side chain is deleted. Figure 4c shows that peak 2 is suppressed in the mechanical unbinding of M3. Similar to the mutants M1 and M2, the position and the amplitudes of other peaks are not affected. It is necessary to note that the Lys28(F5)–Asp23(F3) salt bridge is not solely responsible for the force peak 2 in Fig. 3. The deletion of the charge on the Lys28(F5) side chain also eliminates the interactions between Lys28(F5) and Asp23(F1), which are about 50% weaker than the Lys28(F5)–Asp23(F3) contact.

Hence, the mutants M1–M3 pinpoint the origin of the peaks in the WT force–extension curve. In Fig. 3, the maxima 2 ($<f> = 1164 \pm 68$ pN) and 3 ($<f> = 1323 \pm 60$ pN) are associated with the disruption of Lys28–Asp23 intermolecular interactions and the unbinding of the C-terminal hydrophobic patch (Leu34, Met35, Val36), respectively. The smaller peak 1 ($<f> = 829 \pm 47$ pN) is due to the breakage of CHC hydrophobic interactions.

To probe the contribution of backbone HBs to the mechanical stability of Aβ fibril, we designed the mutant M4, in which all partial charges on the backbone acceptor (CO) and donor (NH) groups in the peptide F5 were set to zero (see Methods). Figure 4d, which compares the force–extension curves $<f(z)>$ for the WT and M4, reveals two features. First, except for the vicinity of peak 2 $<f(z)>$ for M4 is lower than the WT unbinding force by $<\Delta f> \gtrsim 300$ pN. Second, the profiles of $<f(z)>$ for the WT and M4 are similar. These observations indicate that the backbone HBs linking F5 to the fibril contribute to all but the second SimZ+ force peaks. Because there are few backbone HBs in the vicinity of Lys28 in the turn region, the impact of HB deletion on the breakage of Lys–Asp contacts is minimal.
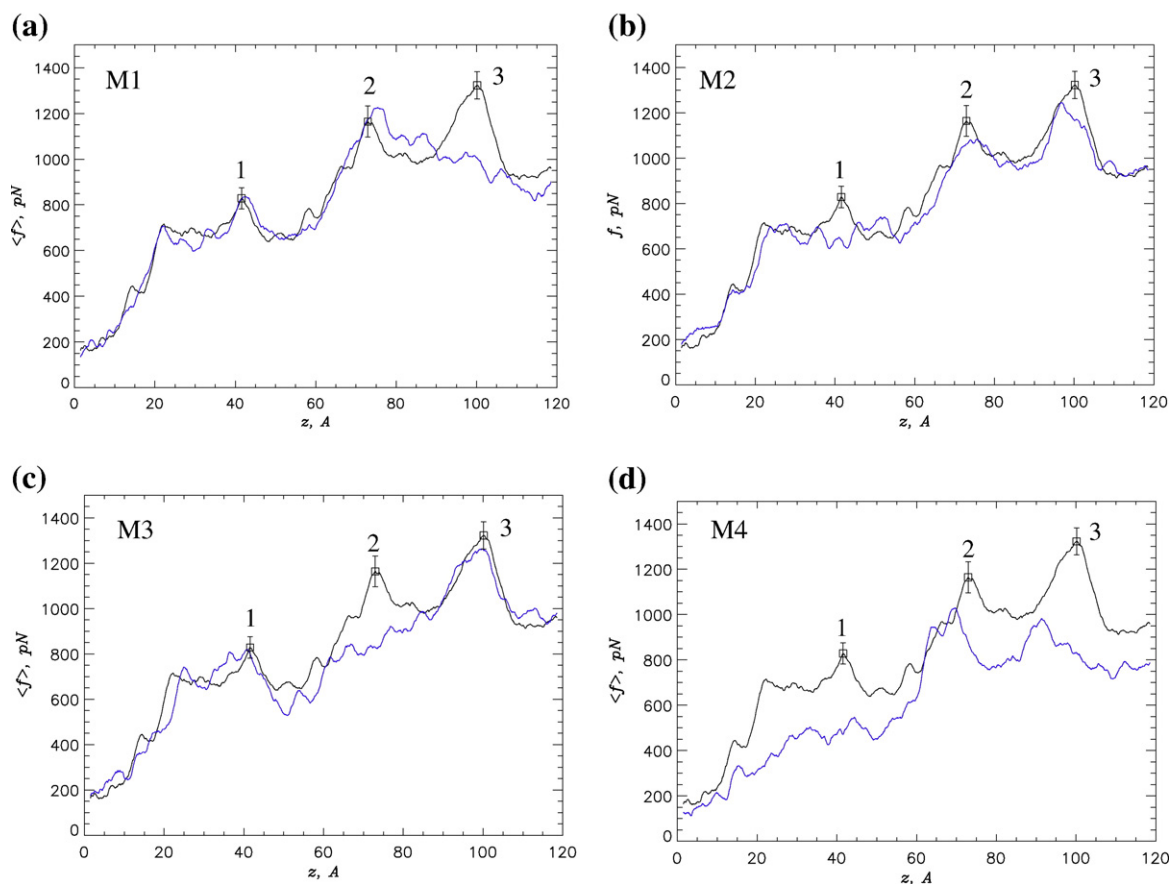
Fig. 4. Comparison of the average force–extension curves $\langle f(z)\rangle$ obtained in SimZ+ simulations for the WT (in black) and the F5 mutants (in blue): (a) M1, (b) M2, (c) M3, and (d) M4. In M1 and M2, the hydrophobic residues in the C terminus or CHC are replaced with glycines, respectively. In M3, the charge on the Lys28 side chain is set to zero. The mutant M4 does not form backbone HBs. The force is averaged over six (WT) or four (mutants) trajectories and smoothed using the sliding window of $\Delta z = 3$ Å. The WT force peaks are marked by the numbers 1–3. The changes observed in $\langle f(z)\rangle$ in response to mutations pinpoint the specific interactions that affect the mechanical unbinding. The force peaks suppressed in (a) and (c) and the overall decrease in $\langle f(z)\rangle$ in (d) indicate that the C-terminal hydrophobic and Lys28–Asp23 electrostatic interactions and backbone HBs determine the mechanical stability of Aβ fibril along its axis.

Lateral mechanical unbinding of Aβ peptides

Figure 5a shows a typical force–extension curve $f(x)$ obtained in the course of lateral unbinding of F5 from the fibril (a SimX+ trajectory, Fig. 1b). Similar to Fig. 2c, this plot reveals distinct force peaks, although their distribution with respect to extension is strikingly different from the SimZ+ results. In particular, the force reaches maximum at the early stages of unbinding. Peak 1 at $x \approx 10$ Å corresponds to the cooperative breakage of in-registry fibril backbone HBs formed by the strand β1. Figure 5b and the inset show that about 12 F5–fibril HBs are cooperatively disrupted at this extension. Interestingly, the number of F5–fibril HBs oscillates until $x \approx 40$ Å, implying that the HBs are repeatedly broken and reestablished albeit in off-registry nonfibril arrangement. Each instance of the breakage of off-registry HBs at $x \approx 15, 22, 30$, and 37 Å results in corresponding force peak, leading to a sawtooth profile (Fig. 5a and b). Once the strand β1 has slid past the fibril ($x \gtrsim 40$ Å), the

force $f(x)$ is reduced as F5 unbinding continues by sequential unzipping of the residues in the strand β2.

The energy of electrostatic interactions $E_{el}(x)$ between Lys28(F5) and Asp23(F3) is plotted in Fig. 5a (inset). The plot demonstrates a complex scenario of Lys28–Asp23 disruption. At $x \approx 20$ Å, when tension reaches Lys28, its side chain changes rotamer conformation. As a result, the salt bridge is partially dissolved. As Lys28 slides past Asp23 (F3), the Lys–Asp salt bridge is transiently reformed before being finally disrupted at $x \approx 37$ Å. Therefore, Lys28(F5)–Asp23(F3) interactions contribute to the peaks 3 and 5 in Fig. 5a. This conclusion is also supported by the simulations of the mutant M3 (see below). Similar to SimZ+ simulations, the electrostatic interactions between Lys28(F5) and Asp23(F1) also make a minor contribution to lateral unbinding.

To evaluate the contribution of hydrophobic interactions, we monitor the disruption of hydrophobic contacts formed by Leu17 and Phe19-Phe20 (from the CHC) and by the C-terminal patch Leu34-Met35-
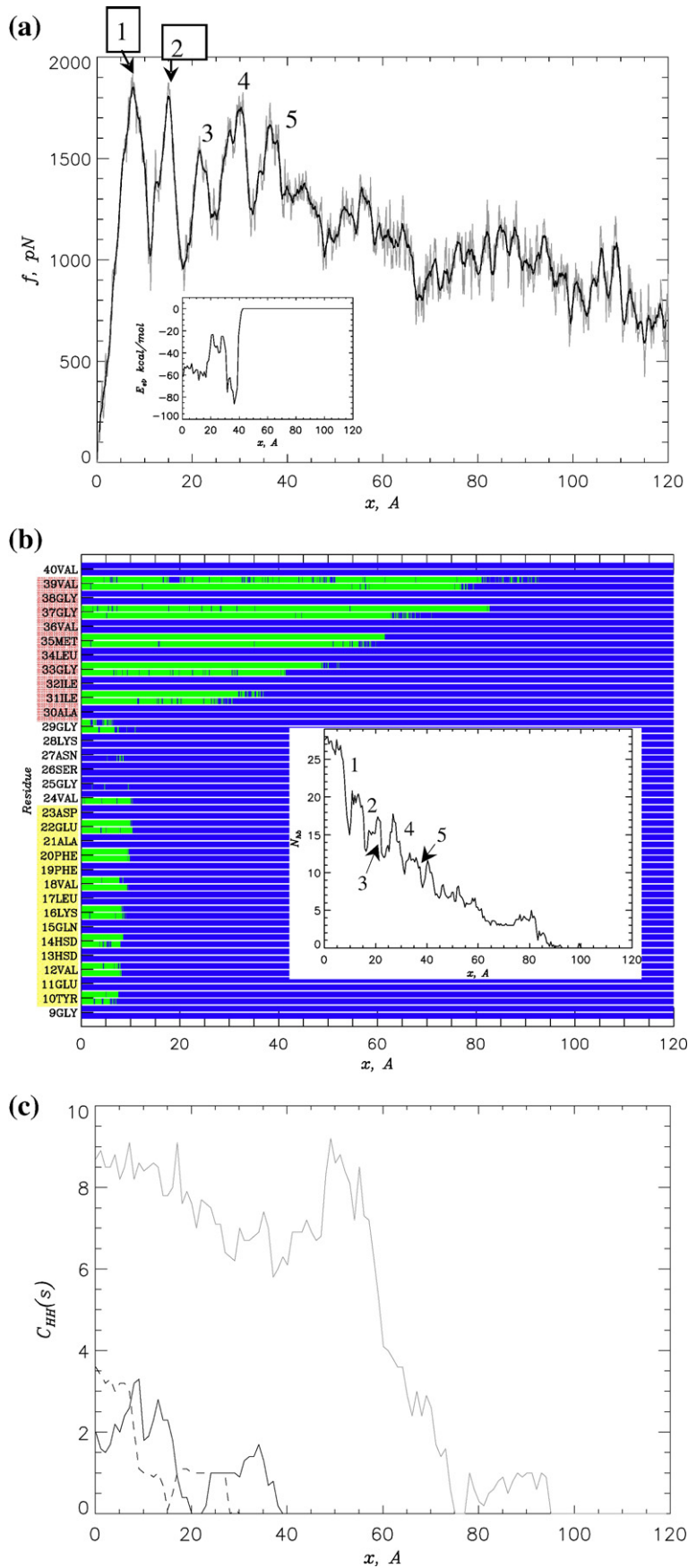
(a)

(b)

(c)

Fig. 5. (a) The force–extension curve $f(x)$ (in grey) describing the unbinding of the peptide F5 in the direction perpendicular to the Aβ fibril axis (Fig. 1b). The thick black line represents the force smoothed using the sliding window of $\Delta x = 3$ Å. The force amplitudes are measured using the smoothed curve. The sawtooth force oscillations at $x < 40$ Å manifest the breakage of fibril in-registry backbone HBs linking F5 to the fibril (peak 1) and subsequent cycles of formation/disruption of off-registry backbone HBs (peaks 2–5) (see also inset to (b)). The inset shows the energy of electrostatic interactions $E_{el}(x)$ between the charged Lys28(F5) and Asp23(F3). $E_{el}(x)$ is smoothed with the sliding window of $\Delta x = 1$ Å. (b) The dynamics of force-induced disruption of the fibril in-registry backbone HBs between the peptides F5 and F3. For each F5 residue there are two horizontal bars, monitoring flickering of HBs formed by NH or CO backbone groups. Green and blue code on and off states, respectively. The inset displays the total number of backbone (in- and off-registry) HBs, $N_{hb}(x)$, formed by the peptide F5 *versus* extension x. The numbers mark the force peaks observed in (a). The residues from the β-strands β1 and β2 are placed in yellow and pink boxes, respectively. (c) The number of hydrophobic contacts $C_{HH}(s)$ *versus* extension x formed by the CHC residues ($s =$ Leu17, dashed line, and $s =$ Phe19-Phe20, in black) and by the C-terminal hydrophobic patch ($s =$ Leu34-Met35-Val36, in grey).

Val36. According to Fig. 5c, the initial loss of fibril-like hydrophobic interactions formed by Leu17 and Phe19-Phe20 occurs at $x \approx 10$ Å and ≈ 15 Å that coincides with the force peaks 1 and 2 in Fig. 5a. Interestingly, the unbinding of the C-terminal hydrophobic patch at $55 \lesssim x \lesssim 75$ Å fails to produce a discernible $f(x)$ peak. Therefore, CHC, but not C terminus, contributes to the force–extension profile. This conjecture is validated below using the mutants M1 and M2.

Figure 3 displays the average unbinding force $\langle f(x) \rangle$ obtained from six independent SimX+ simulations. The plot resembles $f(x)$ for the individual SimX+ trajectory in Fig. 5a. The average force $\langle f(x) \rangle$ is maximum at the early stage of unbinding (peak 1, $\langle f \rangle = 1785 \pm 146$ pN). As in Fig. 5a, a series of sawtooth force peaks is observed. Using the same strategy as in SimZ+ simulations, we link SimX+ force peaks with specific molecular interactions by examining the mechanical unbinding of the mutants M1–M4. Figure 6a compares the average unbinding forces $\langle f(x) \rangle$ for the WT F5 peptide and its M1 mutant. Small deviations in $\langle f(x) \rangle$ are observed at $x \lesssim 50$ Å and within $55 < x < 75$ Å, when the C-terminal hydrophobic contacts are disrupted. However, the change in the amplitude of peak 1 is only 122 pN, which is less than the WT error estimate for this peak. Therefore, the C-terminal hydrophobic patch has a minor impact on the lateral unbinding.

Next, we probe the contribution of CHC residues to the lateral mechanical stability of the fibril. Figure 6b shows the average unbinding force $\langle f(x) \rangle$ for the WT and M2 mutant. The forces generated upon M2 unbinding are noticeably lower than those for the WT. For example, the amplitude of the peak 1 is reduced by about 200 pN to 1581 pN. The lower mechanical stability of M2 is largely observed at $x \lesssim 40$ Å that corresponds to CHC unbinding. Thus, CHC interactions contribute to the lateral stability of Aβ fibril. The mutant M3 (Fig. 6c) probes the impact of the Lys28–Asp23 intermolecular interactions on mechanical unbinding. Despite the deletion of the positive charge on Lys28(F5) side chain the M3 unbinding force $\langle f(x) \rangle$ generally follows that of the WT. For example, the amplitudes of peak 1 are nearly identical (1785 *versus* 1774 pN).
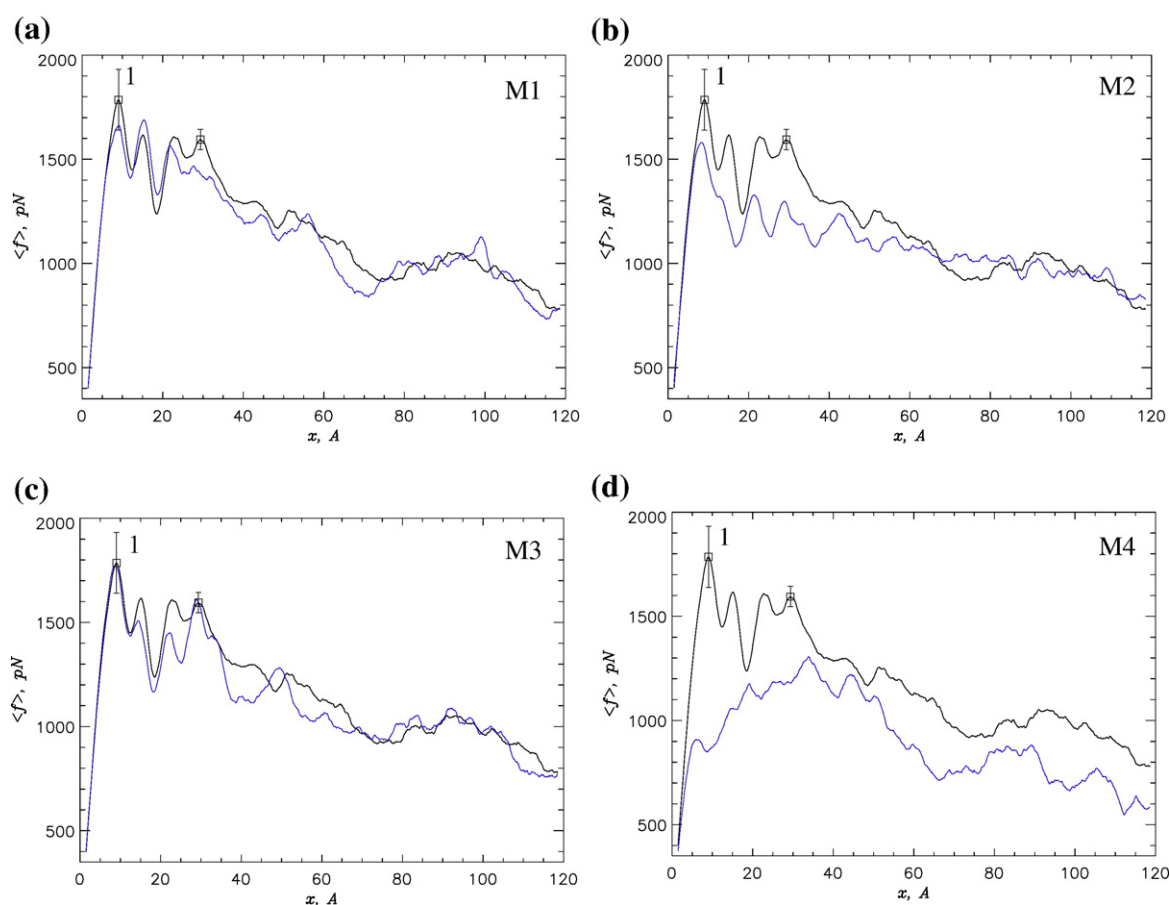
Fig. 6. Comparison of the average force–extension curves $\langle f(x) \rangle$ obtained in SimX+ simulations for the WT (in black) and the F5 mutants (in blue): (a) M1, (b) M2, (c) M3, and (d) M4. The mutants are described in the caption to Fig. 4. The forces are averaged over six (WT) or four (mutants) independent trajectories and smoothed using the sliding window of $\Delta x = 3$ Å. Because the deletion of backbone HBs in M4 (d) dramatically changes the force–extension curve, these interactions are the main contributors to the lateral mechanical stability of Aβ fibril. The dominant force peak 1 is marked in all panels.

Hence, the lateral mechanical unbinding of Aβ is not significantly affected by the Lys28–Asp23 interactions.

To assess the role of backbone HBs we use the mutant M4, in which the formation of backbone HBs is blocked. Figure 6d demonstrates the dramatic effect of the deletion of backbone HBs on the shape and amplitudes of unbinding forces. First, the mutation eliminates the sawtooth force pattern at x <40 Å. This finding confirms that the force variations at x <40 Å are primarily due to the disruption of fibril in-registry backbone HBs and subsequent cycles of formation/rupture of the off-registry F5–F3 HBs. Second, the deletion of HBs drastically reduces the unbinding forces. For instance, the amplitude of peak 1 is decreased in half, from $\langle f \rangle = 1785$ to ≈900 pN.

Discussion

Mechanisms of force-induced unbinding

The simulations SimZ+ and SimX+ probe the mechanical dissociation of the peptides located on the concave edge of Aβ$_{9-40}$ fibril (Fig. 1a and b). To identify the fibril interactions that control the pathways of mechanical unbinding, we analyzed individual pulling trajectories and performed targeted mutations. Figure 3 suggests that the mechanical stability of the edge peptide is highly anisotropic. The threshold mechanical forces observed during the lateral pulling (1785±146 pN) are, on average, 35% higher than those registered during the pulling along the fibril axis (1323±60 pN). Furthermore, both force profiles are strikingly different. The maximum SimX+ forces are reached at the early stages of pulling ($x \lesssim 10$ Å = 0.08L, where L is Aβ$_{9-40}$ contour length). There are also characteristic force oscillations due to repeated formation and breakage of backbone HBs linking the peptide F5 to the fibril. In contrast, SimZ+ simulations display two dominant peaks, 2 and 3, at much larger extensions ($x \gtrsim 0.6L$).

Mechanical unbinding along the fibril axis

Figure 4 reveals the set of fibril interactions involved in the mechanical unbinding along the fibril axis. The force peaks 2 and 3 are completely eliminated upon the deletion of the charge on the Lys28 side chain and the substitution of C-terminal hydrophobic residues in the β2 strand (Leu34, Met35, Val36) with glycines. The backbone fibril HBs also provide significant contribution to the mechanical unbinding. If these HBs are destabilized (the mutant M4), the maximum unbinding force is reduced by 300 pN to ≈1000 pN. Similar level of $f(z)$ would be observed for the double mutant M1+M3, in which Lys positive charge and C-terminal hydrophobic interactions are deleted (Fig. 4a and c). Therefore, the unbinding of Aβ peptides along

the fibril axis is mostly determined by (i) the disruption of Lys-Asp intermolecular contacts, (ii) the breakage of the tethers formed by C-terminal hydrophobic residues (Leu34, Met35, Val36), and (iii) the unzipping of fibril backbone HBs. Interestingly, the CHC in the β1 strand known to be important for Aβ fibril growth[36–39] plays a minor role in the mechanical stability of the edge Aβ peptide.

To rationalize these results, we performed 60-ns constant-temperature (T = 330 K) simulations of the Aβ fibril hexamer shown in Fig. 1a. The peptides F1 and F2 were constrained to the fibril positions, whereas other peptides (F3–F6) remained free. Force was not applied in these simulations. Using the 60-ns trajectory, we computed the average root-mean-square displacement (RMSD) δR_i for the residues i in the peptide F5 with respect to the energy-minimized hexamer structure. (The transformation resulting in minimum RMSD for the entire fibril hexamer was applied before computing δR_i. The values of δR_i were computed using the positions of C$^\alpha$ carbon atoms.) The distribution of δR_i in Fig. 7 reveals dramatic variations in the structural stability within the edge peptide. Few positions in the strands β1 (i = 17–20) and β2 (31–36) are rigid, but the rest (the terminals and the turn) are highly mobile. Interestingly, there are only two β1 residues, Val18 (i = 18) and Phe19 (i = 19), for which δR_i < 1.7 Å. In contrast, five β2 residues have δR_i < 1.7 Å, namely, Ile32, Gly33, Leu34, Met35, and Val36. The average δR_i for the residues in β1 and β2 are 5.2 and 3.0 Å, respectively. Thus, the strand β2 is significantly more rigid than β1. This result is consistent with the greater degree of burial of β2 compared to β1. From the 60-ns trajectory, we found that the average solvent-accessible surface area per residue in β1 is 127 Å^2‡, whereas it is only 95 Å^2 in the strand β2. In addition, according to ProtScale server,[40] the average residue hydrophobicity scores for the strands β1 and β2 are −0.7 and 0.5, respectively§. Taken together, our simulations and these arguments suggest that the C-terminal strand β2 in the edge peptide F5 is mechanically stronger than β1.

Lateral mechanical unbinding

Figure 6 probes the fibril interactions that determine the lateral mechanical stability of Aβ fibril. If backbone HBs are deleted, the maximum unbinding force is reduced by almost 500 pN from 1785 pN for the WT to ≈1300 pN for the mutant M4 (Fig. 6d). Furthermore, the M4 force maximum shifts to larger extensions compared to the WT, and the WT sawtooth force profile is erased. In contrast, the elimination of hydrophobic residues in the C terminus (the mutant M1) and CHC (M2), or of the

---

‡ The first β1 residue, Tyr10, which is highly exposed to solvent, is excluded.

§ Scores are computed using Kyte–Doolittle scale, the window of five residues, and linear weight variation method. The Web address of ProtScale server is http://expasy.org/tools/protscale.html.
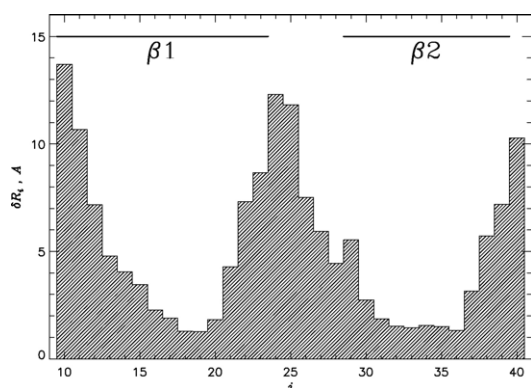
Fig. 7. The distribution of the RMSD values δR_i for the residues i in the edge peptide F5. The values of δR_i represent averages computed from 60 ns equilibrium MD trajectory, in which force was not applied. The distribution of δR_i suggests that the strand β2 is more rigid than β1.

charge on the Lys28 side chain (M3), reduces the maximum force by $\approx$120, 200, and 10 pN, respectively. These results strongly indicate that the dominant factor in the lateral mechanical unbinding is the fibril backbone HBs. As illustrated in the inset to Fig. 5b, more than 10 fibril HBs are broken within $\Delta x \lesssim 2.5$ Å at the early stages of SimX+ simulations ($x \approx 10$ Å). The cooperative HB rupture generates larger unbinding forces than gradual one-by-one unzipping of fibril HBs during the unbinding along the fibril axis (cf. the insets to Figs. 2a and 5b). The dependence of the amplitude of unfolding forces on the pulling direction has been previously noted in theoretical,[41] computational,[42,43] and experimental[44] studies of mechanical unfolding of β-sheet proteins. Furthermore, recent AFM experiments of McAllister *et al.*[23] and Krasnoslobodtsev *et al.*[24] have demonstrated that the forces of rupturing Aβ dimers depend on the location of chain tethering. When the Aβ peptide is immobilized at several chain locations, the average dissociation force was about 300 pN at pH 2.[23] However, if tethering is restricted to the Aβ N terminus, the force decreases to $\approx$41 pN.[24] These experimental results are consistent with our findings, implicating anisotropic mechanical unbinding.

Applicability of SMD for studying the mechanical dissociation of Aβ fibrils

It is important to investigate the scope of applicability of our SMD simulations. Two particular issues must be addressed: (i) the utility of nonequilibrium SMD simulations and (ii) the dependence of mechanical unbinding pathway on the peptide location within Aβ fibril.

Impact of fast SMD pulling

SMD unbinding simulations are performed in highly nonequilibrium regime,[28,41] in which the pulling speed v_p exceeds the equilibrium unbinding

speed v_{eq} by orders of magnitude (see the next section). It is not *a priori* clear if our SMD simulations probe the underlying energetics of Aβ fibril or merely reflect the force ramping due to high rate of pulling. To test the dependence of mechanical unbinding pathway on pulling speed, we reduced v_p three times, from 10^{-4} Å/fs to 3.3×10^{-5} Å/fs and repeated SimZ+ simulations. Figure 8a compares the average force–extension curve $<f(z)>$ computed for the fast and slow SimZ+ simulations. As expected, the slow pulling speed reduces the unbinding forces.[41] More importantly, it does not significantly alter the distribution or the positions of characteristic unbinding force peaks. Examination of slow-pulling trajectories reveals that the two major peaks are due to the breakage of the Lys28–Asp23 interactions (peak 2) and the disruption of the interpeptide tether formed by the three C-terminal hydrophobic residues (Leu34, Met35, Val36, peak 3). Therefore, the "slow" and "fast" pathways for unbinding along the fibril axis are similar. However, Fig. 8a does indicate that care must be taken in inferring the amplitudes of peaks 2 and 3.

The nonequilibrium SMD pulling has been routinely used in probing the mechanical unfolding of proteins.[27,28] For example, stretching ubiquitin domain with the pulling speed of $v_p = 10^{-4}$ Å/fs (also used in this study) provides the estimates of the contour length of ubiquitin, which agree well with the AFM experimental results obtained using much slower pulling rate.[33] The agreement between AFM data and pulling simulations was also reported for E2lip3 and L proteins[44,45] and I27 domain.[34] Therefore, the SMD simulations reported here are likely to reflect the actual mechanism of mechanical dissociation of Aβ fibrils.

Contribution of solvent friction

It has been pointed out that fast-pulling simulations may pick up the force contribution f_s due to solvent friction.[41] Our SMD simulations introduce two potential sources of friction forces. The first is related to the movement of polypeptide through the water bulk. The second is due to the use of Langevin dynamics (LD) to maintain temperature (see Methods). LD introduces a "virtual" solvent, which damps the motions of polypeptide and water atoms. To estimate the force of LD friction, f_{LD}, we performed SMD simulations for a single Aβ$_{9-40}$ peptide without water. By pulling its N terminus with the speed $v_p = 10^{-4}$ Å/fs for 1 ns, we found that $f_{LD} \approx 260$ pN. Assuming linear scaling of f_{LD} with the number of residues n, the average LD friction force per amino acid is $f_{LD,0} \approx 8$ pN. To estimate the friction force caused by water, f_w, we performed SMD simulations for a single Aβ$_{9-40}$ peptide placed in the water box with periodic boundary conditions. By pulling the N terminus with the speed $v_p = 10^{-4}$ Å/fs for 1 ns, we calculated f_w to be $\approx$623 pN (after subtracting f_{LD}). Assuming linear scaling of f_w with n, the average water friction force per amino acid is $f_{w,0} \approx 19$ pN. Therefore, the total
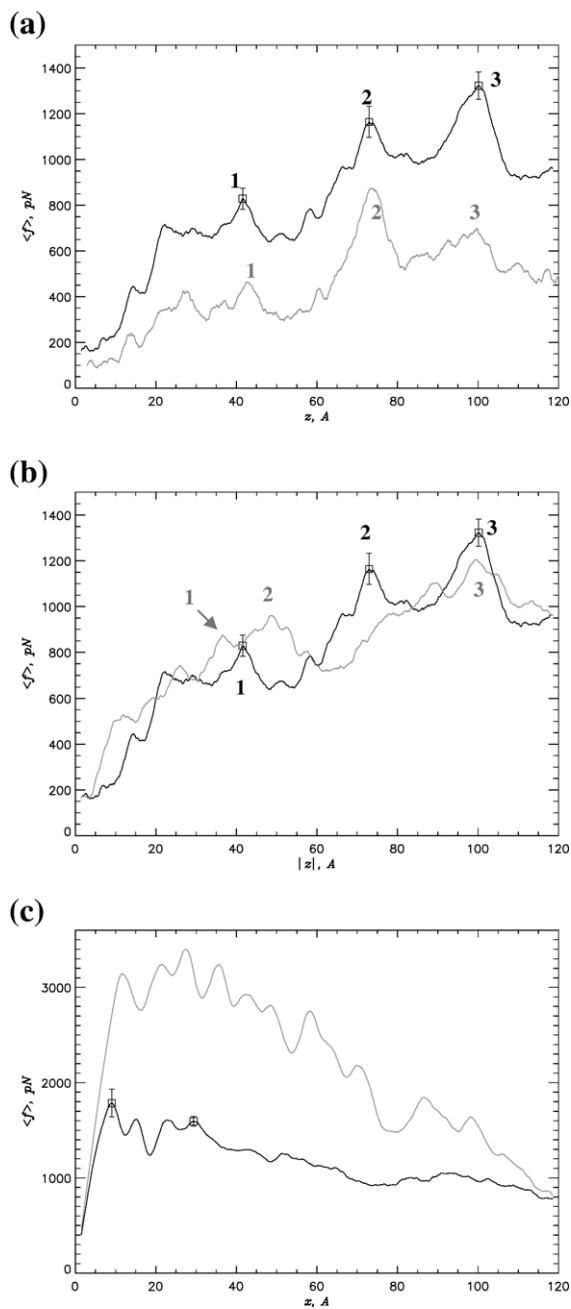
Fig. 8. (a) Comparison of the average force–extension curves $\langle f(z) \rangle$ computed in SimZ+ simulations using two values of the pulling speed v_p: 10^{-4} Å/fs (in black) and 3.3×10^{-5} Å/fs (in grey). (b) Comparison of the average force–extension curves $\langle f(|z|) \rangle$ computed from SimZ+ (in black) and SimZ− (in grey) simulations. SimZ− simulations probe the unbinding from the convex fibril edge. (c) Comparison of the average force–extension curves $\langle f(x) \rangle$ computed in SimX+ simulations for the edge peptide F5 (in black, Fig. 1b) and for the peptide F5 located in the middle of the fibril stack (in grey, Fig. 1c). Apart from the variations in force amplitudes, the unbinding pathways show no significant dependence on the pulling speed or on the precise location of the peptide in Aβ fibril. The forces in grey are averaged over six independent trajectories and smoothed.

friction force acting on F5 peptide in SMD simulations is:

$$fs = n_1 f_{w,0} + n_2 f_{LD,0} \qquad (1)$$

where n_1 is the number of F5 residues moving through the water sphere and n_2 is the number of residues unbound from the fibril. The force f_s is time dependent, because n_1 and n_2 increase with unbinding progress. In SimZ+ simulations, the first F5 residue exits the water sphere at the extension $z \approx 40$ Å, and at $z > 40$ Å n_1 remains constant (≈ 10). The values of n_2 corresponding to the peaks 2 and 3 in Fig. 3 are 20 and 28, respectively. Therefore, according to Eq. (1) the forces f_s for peaks 2 and 3 are 350 and 414 pN, respectively. As a result, the peak forces 2 and 3 in SimZ+ simulations, which are attributed to actual peptide unbinding, are reduced to 814 and 909 pN. In SimX+ simulations the dominant force peak occurs at $x \approx 10$ Å, when approximately 20 F5 residues slide in concert along the fibril edge. (Because the solvent-accessible surface area of the peptide F5 sliding along the fibril is reduced roughly in half compared to fully solvated F5 in the water bulk, $f_{w,0} \approx 9$ pN) Therefore, for the SimX+ force peak 1, $n_1 \approx n_2 \approx 20$ and $f_s \approx 350$ pN. Consequently, the actual force of peptide unbinding in the lateral direction is about 1435 pN. Therefore, given the high rate of mechanical pulling, solvent friction may contribute up to a third of the observed unbinding forces. It is important to note that the friction corrections do not affect the main conclusions of our study (see Conclusions), namely, (i) strong anisotropy of mechanical fibril dissociation and (ii) high mechanical stability of amyloid fibrils compared to typical protein domains.

The estimates of f_s are approximate and do not include such factors as residual hydration of the peptide F5 after its partial extraction from the water sphere or breakage of HBs between the water molecules bound to the peptide and those remaining in the water sphere. For these reasons, the forces recorded at the end of stretching simulations may deviate from the estimates of f_s.

Dependence of mechanical unbinding pathway on the location of peptide in Aβ fibril

It is possible that the location of Aβ peptide in the fibril affects its mechanical unbinding. Indeed, due to the staggering shift of the inner β-sheets[5] the Aβ fibril (Fig. 1a–c) has concave and convex edges. The peptides located on these edges form slightly different set of interactions with the fibril. For example, from the SimZ+ trajectories we obtained that before unbinding a typical hydrophobic residue in the strands β1 and β2 of the peptide F5 (the concave edge in Fig. 1) forms, on an average, 1.5 and 2.4 side-chain hydrophobic peptide–fibril contacts, respectively. For comparison, SimZ− simulations (see below) show that a typical hydrophobic residue in β1 and β2 of the peptide F1 (the convex edge) is engaged in 2.0 and 1.6 peptide–fibril contacts, respectively. However, both peptides F1 and F5

form almost equal numbers of peptide–fibril backbone HBs. Therefore, although the lateral unbinding is unlikely to depend on the location of the edge peptide, such dependence may occur in the unbinding along the fibril axis.

To test this possibility we performed SimZ− simulations, in which the N terminus of the peptide F1 was pulled along the −z direction‖. Figure 8b compares the average unbinding forces $\langle f(|z|)\rangle$ for SimZ+ and SimZ− simulations. In general, the amplitudes and positions of force peaks are fairly similar. A decrease in peak 3 is related to the weaker coupling of the strand β2 to the fibril on the convex edge. The only notable change is the shift of peak 2 from $|z| \approx 70$ Å (SimZ+) to ≈ 50 Å (SimZ−). The analysis of individual SimZ− trajectories indicates that the peak at 50 Å occurs when the salt bridge Asp23(F1)–Lys28(F3) breaks. Because Asp23 is positioned closer to the N terminus than Lys28, the force peak related to the breakage of the salt bridge occurs at the smaller extension. We also repeated SimZ+ simulations, in which the N terminus of the peptide F6 was pulled along the +z direction (Fig. 1a). Because both peptides F5 and F6 are located on the same (concave) fibril edge, one may expect that their mechanical unbindings are similar. Our simulations do confirm that their force–extension curves are nearly identical (data not shown). The simulations, in which the N terminus of F5 (Fig. 1a) was pulled along the +y direction, did not reveal qualitative differences either compared to SimZ+.

Finally, we probed the mechanical unbinding of the peptide located not on the edge, but in the middle of the fibril stack. To examine the force–extension behavior we considered a 10-peptide system (Fig. 1c). Four peptides located on the concave (F9, F10) and convex (F1, F2) edges were constrained to their fibril positions, while six "middle" peptides were free. We repeated the SimX+ simulations, in which the N terminus of the middle peptide F5 was pulled in the lateral (+x) direction (Fig. 1c). The corresponding force–extension plot $\langle f(x)\rangle$ in Fig. 8c reveals two features. First, because the number of peptide–fibril interactions is roughly doubled compared to the edge F5 peptide, the amplitudes of unbinding forces increase nearly twofold (from 1785 to ≈ 3399 pN). Second, the force–extension dependence is generally similar to that observed for the edge peptide in SimX+ simulations. In particular, the maximum unbinding forces, although somewhat shifted to the right, are still reached at relatively small extensions, $x \lesssim 26$ Å $= 0.22L$, where L is Aβ9–40 contour length. Similar to the edge peptide, the maximum unbinding force is related to the cooperative breakage of up to 20 backbone HBs between F5 and the fibril (data not shown). The oscillation of $\langle f(x)\rangle$ at $x < 40$ Å reflects the cycles of formation and breakage of off-registry backbone HBs. To directly evaluate the contribution of backbone HBs we repeated SimX+ stack simulations for the mutant M4, in which the formation of backbone HBs is blocked. Compared to the WT, the maximum unbinding force was reduced by 30% and the oscillation of $\langle f(x)\rangle$ at $x < 40$ Å was erased. Therefore, as for the edge peptide, the rupture of backbone HBs dominates the lateral stretching of the middle peptide.

Hence, we conclude that with some variations, the pathways of mechanical unbinding mapped in SimZ+ and SimX+ simulations appear to be applicable to concave and convex edges of Aβ fibril and to the peptides stacked in its middle.

Comparison of mechanical stabilities of amyloid fibrils and protein domains

Using our simulations we can estimate the equilibrium force f_{eq} required for unbinding Aβ peptide from the fibril. Assuming that our pulling speed v_p is much faster than the equilibrium unbinding speed v_{eq}, we use the relationship:[41]

$$f \simeq f_{eq} \ln \frac{v_p}{v_{eq}} \qquad (2)$$

where f is the maximum nonequilibrium unbinding force. To estimate v_{eq} we use $v_{eq} \simeq Lk_d$, where $L = 118$ Å is the contour length of Aβ9–40 peptide and k_d is the dissociation rate. Identifying k_d with the slow dissociation rate constant measured by Esler *et al.* for the peptide "locked" in the fibril,[46] we set k_d $\sim 10^{-3}$ min^{-1}. Using the SimZ+ maximum force $\langle f \rangle \approx 1323$ pN and $v_p = 10^{-4}$ Å/fs and subtracting the friction correction $f_s \approx 414$ pN [Eq. (1)], we find that $f_{eq} \approx 29$ pN. Because lateral unbinding generates larger threshold forces, this estimate of f_{eq} represents the lower bound. A similar estimate can be made using the AFM data of McAllister *et al.*[23] Their study measured the forces of dissociating Aβ dimers induced to adopt β-structure by low pH. Using their experimental parameters ($v_p = 0.25$ μm/s and f ≈ 300 pN) we get $f_{eq} \approx 21$ pN. The estimates of f_{eq} contain two implications. First, our SMD simulations and AFM experiments[23] give fairly consistent values of equilibrium forces of dissociating Aβ β-structure. This suggests that SMD simulations indeed measure the mechanical stability of Aβ fibrils. Second, f_{eq} obtained for Aβ fibril corresponds to the upper limit of experimental unfolding f_{eq} obtained for immunoglobulin (Ig) domains. For example, f_{eq} for proximal and distal Ig domains span the range from ≈ 5 to 30 pN.[47] Ig domains are mechanically active and represent one of the most force-resistant protein folds.[48] This comparison suggests that Aβ fibrils are mechanically stronger than most protein domains.

Conclusions

In summary, our MD simulations studied the pathways of mechanical dissociation of Aβ9–40

‖ In contrast to SimZ+, in SimZ− simulations the peptides F5 and F6 were constrained, whereas F1–F4 were free.

peptides from amyloid fibrils in longitudinal and lateral directions with respect to the fibril axis. By examining the force-induced unbinding of the peptides located on distinct fibril edges or stacked in the middle of the fibril protofilament, we determined that the computed pathways are roughly independent on the precise location of the peptide in the fibril. More specifically, our study leads us to the following conclusions:

(1) The force required to mechanically unbind Aβ peptide in the lateral direction is larger than that registered along the fibril axis.

(2) The maximum force in lateral unbinding is reached by stretching the peptide by merely $\sim 0.08L$, where L is Aβ contour length. In contrast, the maximum force during the unbinding along the fibril axis is reached at much larger extensions ($\gtrsim 0.6L$). Therefore, the edge Aβ peptide is brittle in the lateral direction but is "soft" when pulled along the fibril axis.

(3) The lateral mechanical unbinding and the unbinding along the fibril axis load different sets of fibril interactions. The lateral unbinding is primarily determined by the cooperative rupture of fibril backbone HBs. In contrast, the unbinding along the fibril axis depends on the combination of intrafibril interactions, including interpeptide Lys–Asp electrostatic contacts, the hydrophobic interactions formed by the Aβ C terminus, and fibril backbone HBs.

(4) Mechanical stability of Aβ fibrils is not significantly affected by the CHC interactions. It is known that the substitution of CHC phenylalanines with less hydrophobic residues sharply slows down amyloid formation.[36] Assuming the reversibility of temperature-induced deposition/dissociation[19] we propose that the pathways of force and temperature-induced unbinding are different. This conclusion is consistent with the protein unfolding studies, which showed the divergence of mechanical and thermal denaturation paths in the limit of strong forces.[49–51]

(5) Because all amyloid fibrils incorporate extensive β-sheet structure, the anisotropic mechanical dissociation of Aβ fibrils is likely to be relevant to other amyloid assemblies. The mechanical "fingerprints" of Aβ fibrils reported here may potentially be used in AFM experiments to detect ordered β-structure regions in amyloid fibrils or to probe their orientation.

Because the N terminus of Aβ peptide can be functionalized and recognized by AFM probe, we applied force to the N-terminal Gly9 residue. However, similar to forced unfolding of proteins, mechanical unbinding is expected to depend on the point of force application.[43] Therefore, the pathways reported here are applicable to the case when mechanical force acts on the Aβ N terminus. Finally, the estimates of equilibrium forces required to unbind Aβ peptide from the amyloid fibril indicate that these supramolecular structures are mechanically stronger than most protein domains. High mechanical stability of amyloids also reported in recent experimental studies[25,52] makes these assemblies attractive for biotechnological applications.

Methods

Simulations of mechanical unbinding of Aβ peptides were performed using the Aβ$_{9–40}$ fibril structure of Petkova et al.[5] Using solid-state NMR, these authors have derived the positions of all residues of Aβ$_{1–40}$ peptide in the fibril except for the first eight disordered N-terminal amino acids.[16,53] Here, we use the hexamer fragment of Aβ$_{9–40}$ fibril (Fig. 1) solvated in a water sphere with the radius $R_s = 49$ Å and the density of 1.00 g/cm^3. In all, the system contains 48,336 atoms. Using NAMD program[54] and CHARMM22 force field, we heated the system to 330 K and equilibrated it for 300 ps. To maintain water density and sphere shape during heating and equilibration, spherical boundary conditions were applied to water molecules. The aim of the simulations was to investigate the force-induced unbinding of the edge Aβ peptides from the fibril. Consequently, to mimic the stability of the "bulk" fibril, the backbone heavy atoms of the peptides F1 and F2 (Fig. 1a and b) were constrained to their fibril positions at all simulation stages. During heating and equilibration the peptides F3–F6 were constrained to fibril positions using soft harmonic springs. These constraints were released once equilibration was completed.

The force-induced unbinding of Aβ peptides was studied using SMD mode in the NAMD program. The temperature of 330 K during SMD was maintained using Langevin dynamics with the damping coefficient 5 ps^{-1}. The retaining point[55] was attached to the C$^\alpha$ atom of the N-terminal residue Gly9 of the peptide F5 (Fig. 1) using harmonic spring with the constant $k_r = 6.6$ kcal/(mol Å^2). The retaining point was pulled with the constant speed $v_p = 10^{-4}$ Å/fs in two directions. In SimZ+ simulations the retaining point was pulled along the $+z$ direction parallel with the fibril axis (Fig. 1a). In SimX+, the pulling occurred along the $+x$ direction perpendicular to the fibril axis (Fig. 1b). For each direction, we obtained six independent 1.2-ns trajectories, resulting in complete unbinding of Aβ peptide from the fibril. To compare the conformation of the edge peptide F5, with which SMD pulling was initiated, with the F5 experimental fibril structure we computed the RMSD using the positions of Ca carbon atoms. The average RMSD for F5 residues in the initial SMD structures is ≈ 0.5 Å. Hence, the initial conformations of the edge peptides in the SMD simulations closely resemble the structures of Aβ$_{9–40}$ peptides inside the fibril. Note also that during SMD simulations there is little change in the conformations of the middle peptides F3 and F4 (Fig. 1a). For example, the average RMSD for F3 residues during 1.2-ns SMD trajectory is 1.1 Å.

The following rationale was used to determine the point of force application in the Aβ chain. Because the Aβ N terminus is disordered in the fibril,[5,16,53] it can be chemically modified to facilitate the bonding between the peptide and the tip of AFM cantilever without perturbing the structure of the fibril. One of the possibilities is to attach a glutaraldehyde anchor to the amino terminus of the Aβ peptide.[23] An alternative is to use polyethylene glycol (PEG) linkers.[20] It has been demonstrated that the structures of fibril protofilaments for PEG-Aβ copolymers and

WT Aβ are similar.[56] Importantly, recent AFM experiments have utilized maleimide-PEG tethers, which were specifically attached to the cystine modified N termini of Aβ$_{1-40}$.[24] These arguments suggest that the N terminus is an appropriate site for force application in SMD.

Previous studies have revealed the dependence of mechanical unfolding of proteins on the direction of external force.[43,44] In particular, protein structure is mechanically stronger if force is applied parallel with the β-strands in a β-sheet compared to the case when tension is applied in the perpendicular direction with respect to β-strands. Because the direction of AFM tip retraction with respect to Aβ fibril is not *a priori* known, we applied the force in two orthogonal directions, one along the fibril axis (SimZ+) and the other perpendicular to the fibril axis (SimX+). We have also tested if the mechanical unbinding depends on the specific location of Aβ peptide in the fibril. To this end, we performed SMD simulations for the peptides F1 and F6 (Fig. 1a) and for the peptide located in the middle of the fibril stack (Fig. 1c).

In order to distinguish the contributions of various molecular interactions to mechanical stability of Aβ fibrils, several mutants of the peptide F5 were designed. The mutants M1 and M2 probe the contribution of hydrophobic interactions formed by the Aβ C terminus and the CHC. In M1 we replaced three hydrophobic residues (Leu34, Met35, and Val36) in the Aβ C terminus with glycines. M2 was obtained by substituting Leu17, Phe19, and Phe20 from the CHC with glycines. To test the importance of electrostatic contacts formed by Lys28(F5) (Fig. 1a), we created the mutant M3, in which the charge on Lys28 side chain was deleted. Finally, we designed the mutant M4, in which all partial charges on the backbone acceptor (CO) and donor (NH) groups in the peptide F5 were set to zero. M4 was used to evaluate the contribution of backbone HBs to mechanical stability of the fibril. For each mutant, we repeated SimZ+ and SimX+ simulations at least four times.

The mechanism of mechanical dissociation was characterized by the dependence of the resisting force generated in the spring connecting the peptide and the retaining point on the extension. The extension is defined as follows. At the start of SMD simulation, the position of retaining point coincides with the position of the Aβ N terminus. During SMD simulations, the retaining point is moved with the constant speed v_p along the $+z$ or $+x$ directions. The distance between the current position of the retaining point and its position at the start of SMD represents the extension z or x. In addition, we computed the number of side-chain contacts as described in our early studies.[57] Backbone HBs between the peptide and the fibril were assigned according to Kabsch and Sander.[58] The potential energy between atom groups was computed using the mdenergy module from VMD package.[59] The distribution of water molecules near the fibril was obtained using pair correlation functions $g(r)$.[60] Throughout the paper, angular brackets (<..>) imply averaging over multiple independent trajectories.

The simulation system consists of the fibril hexamer centered in the water sphere. Because no boundary conditions were applied to water molecules during SMD mode, they may diffuse out of the sphere or be dragged by the peptide retracted from the fibril. Indeed, by the end of SMD trajectory two-thirds of the peptide is extended beyond the boundary of the water sphere. To check the density of water, we compared the average number of water molecules in the fibril first solvation shells in the SMD simulations and in the separate simulations, in which the spherical boundary condition (SBC) was always applied to water molecules. We found that during the 1.2-ns SMD trajectory the first solvation shell water density was, on average, 3% lower than in the simulations with SBC. Therefore, the absence of SBC in short SMD simulations does not significantly affect the water density near the fibril. Note that SBC cannot be applied to water during SMD mode because it would result in false peaks in force–extension plots.

References

1. Dobson, C. M. (2003). Protein folding and misfolding. *Nature*, **426**, 884–890.
2. Serpell, L. C. (2000). Alzheimer's amyloid fibrils: structure and assembly. *Biochim. Biophys. Acta*, **1502**, 16–30.
3. Burkoth, T. S., Benzinger, T., Urban, V., Morgan, D. M., Gregory, D. M., Thiyagarajan, P. *et al.* (2000). Structure of the β-amyloid(10–35) fibril. *J. Am. Chem. Soc.* **122**, 7883–7889.
4. Lakdawala, A. S., Morgan, D. M., Liotta, D. C., Lynn, D. G. & Snyder, J. P. (2002). Dynamics and fluidity of amyloid fibrils: a model of fibrous protein aggregates. *J. Am. Chem. Soc.* **124**, 15150–15151.
5. Petkova, A. T., Yau, W.-M. & Tycko, R. (2006). Experimental constraints on quaternary structure in Alzheimer's β-amyloid fibrils. *Biochemistry*, **45**, 498–512.
6. Luhrs, T., Ritter, C., Adrian, M., Loher, B., Bohrmann, D. R., Dobeli, H. *et al.* (2005). 3D structure of Alzheimers amyloid-β(1–42) fibrils. *Proc. Natl. Acad. Sci. USA*, **102**, 17342–17347.
7. Nelson, R., Sawaya, M. R., Balbirnie, M., Madsen, A. O., Riekel, C., Grothe, R. & Eisenberg, D. (2005). Structure of the cross-β spine of amyloid-like fibrils. *Nature*, **435**, 773–778.
8. Makin, O. S., Atkins, E., Sikorski, P., Johansson, J. & Serpell, L. C. (2005). Molecular basis for amyloid fibril formation and stability. *Proc. Natl. Acad. Sci. USA*, **102**, 315–320.
9. Ferguson, N., Becker, J., Tidow, H., Tremmel, S., Sharpe, T. D., Krause, G. *et al.* (2006). General structural motifs of amyloid protofilaments. *Proc. Natl. Acad. Sci. USA*, **103**, 16248–16253.
10. Hamada, D. & Dobson, C. M. (2002). A kinetic study of β-lactoglobulin amyloid fibril formation promoted by urea. *Prot. Sci.* **11**, 2417–2426.
11. Benzinger, T., Gregory, D. M., Burkoth, T. S., Miller-Auer, H., Lynn, D. G., Botto, R. E. & Meredith, S. C. (2000). Two-dimensional structure of β-amyloid(10–35) fibrils. *Biochemistry*, **39**, 3491–3499.
12. Antzutkin, O. N., Balbach, J. J., Leapman, R. D., Rizzo, N. W., Reed, J. & Tycko, R. (2000). Multiple quantum solid-state NMR indicates a parallel, not antiparallel, organization of β-sheets in Alzheimer's β-amyloid fibrils. *Proc. Natl. Acad. Sci. USA*, **97**, 13045–13050.

13. Antzutkin, O. N., Leapman, R. D., Balbach, J. J. & Tycko, R. (2002). Supramolecular structural constraints on Alzheimers β-amyloid fibrils from electron microscopy and solid-state nuclear magnetic resonance. *Biochemistry,* **41**, 15436–15450.

14. Ma, B. & Nussinov, R. (2002). Stabilities and conformations of Alzheimer's β-amyloid peptide oligomers (Aβ$_{16-22}$, Aβ$_{16-35}$, and Aβ$_{10-35}$): sequence effects. *Proc. Natl. Acad. Sci. USA,* **99**, 14126–14131.

15. Williams, A. D., Portelius, E., Kheterpal, I., Guo, J., Cook, K., Xu, Y. & Wetzel, R. (2004). Mapping Aβ amyloid fibril secondary structure using scanning proline mutagenesis. *J. Mol. Biol.* **335**, 833–842.

16. Petkova, A. T., Ishii, Y., Balbach, J. J., Antzutkin, O. N., Leapman, R. D., Delaglio, F. & Tycko, R. (2002). A structural model for Alzheimer's β-amyloid fibrils based on experimental constraints from solid state NMR. *Proc. Natl. Acad. Sci. USA,* **99**, 16742–16747.

17. Ma, B. & Nussinov, R. (2006). Simulations as analytical tools to understand protein aggregation and predict amyloid conformation. *Curr. Opin. Struct. Biol.* **10**, 445–452.

18. Buchete, N.-V., Tycko, R. & Hummer, G. (2005). Molecular dynamics simulations of Alzheimers β-amyloid protofilaments. *J. Mol. Biol.* **353**, 804–821.

19. Takeda, T. & Klimov, D. K. (2007). Dissociation of abeta16–22 fibrils probed by molecular dynamics. *J. Mol. Biol.* **368**, 1202–1213.

20. Ray, C. & Akhremitchev, B. B. (2005). Conformational heterogeneity of surface-grafted amyloidogenic fragments of alpha-synuclein dimers detected by atomic force microscopy. *J. Am. Chem. Soc.* **127**, 14739–14744.

21. Guo, S. & Akhremitchev, B. B. (2006). Packing density and structural heterogeneity of insulin amyloid fibrils measured by AFM nanoindentation. *Biomacromolecules,* **7**, 1630–1636.

22. Kellermayer, M. S. Z., Grama, L., Karsai, A., Nagy, A., Kahn, A., Datki, Z. L. & Penke, B. (2005). Reversible mechanical unzipping of amyloid β-fibrils. *J. Biol. Chem.* **280**, 8464–8470.

23. McAllister, C., Karymov, M. A., Kawano, Y., Lushnikov, A. Y., Mikheikin, A., Uversky, V. N. & Lyubchenko, Y. L. (2005). Protein interactions and misfolding analyzed by AFM force spectroscopy. *J. Mol. Biol.* **354**, 1028–1042.

24. Krasnoslobodtsev, A. V., Shlyakhtenko, L. S., Ukraintsev, E., Zaikova, T. O., Keana, J. F. W. & Lyubchenko, Y. L. (2005). Nanomedicine and protein misfolding diseases. *Nanomedicine,* **1**, 300–305.

25. Smith, J. F., Knowles, T. P. J., Dobson, C. M., MacPhee, C. E. & Welland, M. E. (2006). Characterization of the nanoscale properties of individual amyloid fibrils. *Proc. Natl. Acad. Sci. USA,* **103**, 15806–15811.

26. Karsai, A., Martonfalvi, Z., Nagy, A., Grama, L., Penke, B. & Kellermayer, M. S. Z. (2006). Mechanical manipulation of Alzheimer's amyloid β1–42 fibrils. *J. Struct. Biol.* **155**, 316–326.

27. Isralewitz, B., Gao, M. & Schulten, K. (2001). Steered molecular dynamics and mechanical functions of proteins. *Curr. Opin. Struct. Biol.* **11**, 224–230.

28. Isralewitz, B., Baudry, J., Gullingsrud, J., Kosztin, D. & Schulten, K. (2001). Steered molecular dynamics investigations of protein function. *J. Mol. Graphics Modell.* **19**, 13–25.

29. Lu, H. & Schulten, K. (1999). Steered molecular dynamics simulation of conformational changes of immunoglobulin domain I27 interpret atomic force microscopy observations. *Chem. Phys.* **247**, 141–153.

30. Paci, E. & Karplus, M. (2000). Unfolding proteins by external forces and temperature: the importance of topology and energetics. *Proc. Natl. Acad. Sci. USA,* **97**, 6521–6526.

31. Craig, D., Krammer, A., Schulten, K. & Vogel, V. (2001). Comparison of the early stages of forced unfolding for fibronectin type III modules. *Proc. Natl. Acad. Sci. USA,* **98**, 5590–5595.

32. Gao, M., Craig, D., Lequin, O., Campbell, I. D., Vogel, V. & Schulten, K. (2003). Structure and functional significance of mechanically unfolded fibronectin type III1 intermediates. *Proc. Natl. Acad. Sci. USA,* **100**, 14784–14789.

33. Carrion-Vazquez, M., Li, H., Lu, H., Marszalek, P. E., Oberhauser, A. F. & Fernandez, J. M. (2003). The mechanical stability of ubiquitin is linkage dependent. *Nat. Struct. Biol.* **10**, 738–743.

34. Best, R. B., Fowler, S. B., Herrera, J. L. T., Steward, A., Paci, E. & Clarke, J. (2003). Mechanical unfolding of a titin Ig domain: structure of transition state revealed by combining atomic force microscopy, protein engineering and molecular dynamics simulations. *J. Mol. Biol.* **330**, 867–877.

35. Li, P.-C. & Makarov, D. E. (2004). Ubiquitin-like protein domains show high resistance to mechanical unfolding similar to that of the I27 domain in titin: evidence from simulations. *J. Phys. Chem. B,* **108**, 745–749.

36. Chiti, F., Stefani, M., Taddei, N., Ramponi, G. & Dobson, C. M. (2003). Rationalization of the effects of mutations on peptide and protein aggregation rates. *Nature,* **424**, 805–808.

37. Chalifour, R. J., McLaughlin, R. W., Lavoie, L., Morissette, C., Tremblay, N., Boule, M. *et al.* (2003). Stereoselective interactions of peptide inhibitors with the β-amyloid peptide. *J. Biol. Chem.* **278**, 34874–34881.

38. Gordon, D. J. & Meredith, S. C. (2003). Probing the role of backbone hydrogen bonding in β-amyloid fibrils with inhibitor peptides containing ester bonds at alternate positions. *Biochemistry,* **42**, 475–485.

39. de Groot, N. S., Pallars, I., Avils, F. X., Vendrell, J. & Ventura, S. (2005). Prediction of hot spots of aggregation in disease-linked polypeptides. *BMC Struct. Biol.* **5**, 18–33.

40. Gasteiger, E., Hoogland, C., Gattiker, A., Duvaud, S., Wilkins, M. R., Appel, R. D. & Bairoch, A. (2005). Protein identification and analysis tools on the ExPASy server. In *The Proteomics Protocols Handbook* (Walker, J. M., ed) pp. 571–607, Humana Press, Totowa, NJ.

41. Evans, E. (2001). Probing the relation between force—lifetime—and chemistry in single molecular bonds. *Annu. Rev. Biophys. Biomol. Struct.* **30**, 105–128.

42. Klimov, D. K. & Thirumalai, D. (2000). Native topology determines force-induced unfolding pathways in globular proteins. *Proc. Natl. Acad. Sci. USA,* **97**, 7254–7259.

43. West, D. K., Brockwell, D. J., Olmsted, P. D., Radford, S. E. & Paci, E. (2006). Mechanical resistance of proteins explained using simple molecular models. *Biophys. J.* **90**, 287–297.

44. Brockwell, D. J., Paci, E., Zinober, R. C., Beddard, G. S., Olmsted, P. D., Smith, D. A. *et al.* (2003). Pulling geometry defines the mechanical resistance of a β-sheet protein. *Nat. Struct. Biol.* **10**, 731–737.

45. Brockwell, D. J., Beddard, G. S., Paci, E., West, D. K., Olmsted, P. D., Smith, D. A. & Radford, S. E. (2005). Mechanically unfolding the small, topologically simple protein L. *Biophys. J.* **89**, 506–519.

46. Esler, W. P., Stimson, E. R., Jennings, J. M., Vinters, H. V., Ghilardi, J. R., Lee, J. P. *et al.* (2000). Alzheimer's disease amyloid propagation by a template-dependent dock–lock mechanism. *Biochemistry*, **39**, 6288–6295.

47. Li, H., Linke, W. A., Oberhauser, A. F., Carrion-Vazquez, M., Kerkvliet, J. G., Lu, H. *et al.* (2002). Reverse engineering of the giant muscle protein titin. *Nature*, **418**, 998–1002.

48. Forman, J. R. & Clarke, J. (2007). Mechanical unfolding of proteins: insights into biology, structure and folding. *Curr. Opin. Struct. Biol.* **17**, 58–66.

49. Huang, S., Ratliff, K. S., Schwartz, M. P., Spenner, J. M. & Matouschek, A. (1999). Mitochondria unfold precursor proteins by unraveling them from their N-termini. *Nat. Struct. Biol.* **6**, 1132–1138.

50. Tian, P. & Andricioaei, I. (2005). Repetitive pulling catalyzes cotranslocational unfolding of barnase during import through a mitochondrial pore. *J. Mol. Biol.* **350**, 1017–1034.

51. Williams, P. M., Fowler, S. B., Best, R. B., Toca-Herrera, J. L., Scott, K. A., Steward, A. & Clarke, J. (2003). Hidden complexity in the mechanical properties of titin. *Nature*, **422**, 446–449.

52. Kol, N., Adler-Abramovich, L., Barlam, D., Shneck, R. Z., Gazit, E. & Rousso, I. (2005). Self-assembled peptide nanotubes are uniquely rigid bioinspired supramolecular structures. *Nano Lett.* **5**, 1343–1346.

53. Torok, M., Milton, S., Kayed, R., Wu, P., McIntire, T., Glabe, C. G. & Langen, R. (2002). Structural and dynamical features of Alzheimer's Aβ peptide in amyloid fibrils studied by site-directed spin labeling. *J. Biol. Chem.* **277**, 40810–40815.

54. Kale, L., Skeel, R., Bhandarkar, M., Brunner, R., Gursoy, A., Krawetz, N. *et al.* (1999). NAMD2: greater scalability for parallel molecular dynamics. *J. Comput. Phys.* **151**, 283–312.

55. Lu, H., Isralewitz, B., Krammer, A., Vogel, V. & Schulten, K. (1998). Unfolding of titin immunoglobulin domains by steered molecular dynamics simulations. *Biophys. J.* **75**, 662–671.

56. Lynn, D. G. & Meredith, S. C. (2000). Review: model peptides and the physicochemical approach to β-amyloids. *J. Struct. Biol.* **130**, 153–173.

57. Klimov, D. K. & Thirumalai, D. (2003). Dissecting the assembly of Aβ16–22 amyloid peptides into antiparallel β-sheets. *Structure*, **11**, 295–307.

58. Kabsch, W. & Sander, C. (1983). Dictionary of protein secondary structure: pattern recognition of hydrogen-bonded and geometrical features. *Biopolymers*, **22**, 2577–2637.

59. Humphrey, W., Dalke, A. & Schulten, K. (1996). VMD—visual molecular dynamics. *J. Mol. Graphics*, **14**, 33–38.

60. Klimov, D. K., Straub, J. E. & Thirumalai, D. (2004). Aqueous urea solution destabilizes Aβ16–22 oligomers. *Proc. Natl. Acad. Sci. USA*, **101**, 14760–14765.